Hindawi
International Journal of Aerospace Engineering
Volume 2023, Article ID 5085334, 19 pages
https://doi.org/10.1155/2023/5085334

Research Article

Damage Initiation Analysis of a Tension Stiffened Composite PRSEUS Panel Based on Modified Hashin Criteria

Yongjie Zhang, Samya Ettoumi, Bo Cui, and Jingpiao Zhou

Northwestern Polytechnical University, Xi'an, China 710072

Correspondence should be addressed to Yongjie Zhang; zyj19191@nwpu.edu.cn

Received 4 September 2022; Revised 3 January 2023; Accepted 5 January 2023; Published 23 January 2023

Academic Editor: Zhiguang Song

In this study, a damaged three-stringer PRSEUS panel simulating a midbay-to-midbay damage scenario was modelled in Abaqus and analyzed under tension. Moreover, employing the Abaqus built-in Hashin failure criteria verified the reliability of the criteria in predicting damage initiation with great accuracy. Further, these criteria were implemented via UMAT to investigate the effect of shear stress on the analysis, indicating that manipulating the coefficient of shear stress contribution led to a significant enhancement in analysis accuracy. Lastly, the same procedure was followed in the analysis of a repaired three-stringer panel, validating once again the adequacy of the adopted approach and simultaneously highlighting the efficiency of the repair technique in restoring load carrying of the PRSEUS panel. This study may provide a dependable reference presenting a simplified and significantly less computationally demanding approach for damage analysis composite structures and their repair, in addition to further applying these techniques to access the damage-arresting capabilities of these structures.

1. Introduction

The Environmentally Responsible Aviation (ERA) project [1–6] was developed by NASA to study next-generation flight vehicle configurations. The basic premise of the project is that unconventional, robust, and lightweight structures requiring less fuel consumption and producing fewer pollutants are introduced. These structures eventually play a significant role in reducing the negative effect arising from aviation on the environment. They are considered structurally superior since they are characterized by a higher lift-to-drag ratio, reduced drag, and lower community noise, in addition to reducing the cost of the design, manufacturing, and testing [7]. The Pultruded Rod Stitched Efficient Unitized Structure (PRSEUS) concept, illustrated in Figure 1, is the principal structural concept being developed under the ERA project, by NASA, and Boeing researchers.

The PRSEUS concept comprises dry carbon-epoxy components, foam core, and pultruded rods stitched together into a stiffened panel that is subjected to resin infusion and out-of-autoclave curing. In addition, eliminating the use of fasteners almost entirely results in a weight-efficient structure with considerable crack-arresting capabilities due to through-thickness stitching. As a result, the occurrence of delamination is downscaled, and necessary out-of-plane strength is generated for the structure to ultimately fail as a unit. For more details on the manufacturing process, please refer to [6]. The respective lamina is 1.32 mm thick and comprises 7 plies stacked as the sequence $[45,-45,0,90,0,-45,45]_T$, in which the fiber has percentages of 44.9, 44.9, and 12.2 for 0°, 45°, and 90°, respectively.

Since the research on the potential advantages of the HWB in high-efficiency subsonic travel has aroused extensive attention [8–15], the unique damage-arresting capabilities exhibited by the PRSEUS structure have been investigated under different loading conditions to verify its feasibility and applicability for the Hybrid Wing Body (HWB) airplane [16]. In general, numerical analyses will be conducted to predict the behavior of the panel, whereas experiments would be performed to validate the above predictions and hypotheses. However, testing will require a considerable number of funding if one should study the integrity of a PRSEUS structure in depth; it also will be time-consuming. Accordingly, computer-aided engineering

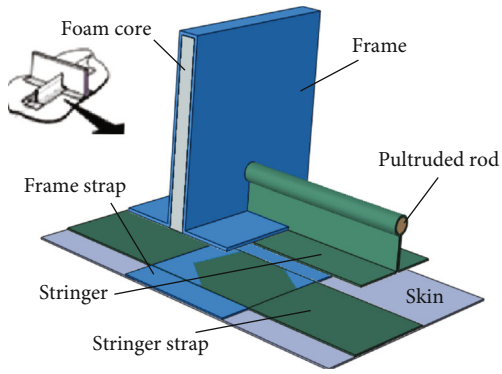

Figure 1: PRSEUS panel's general assembly.

software is considered to be conducive to reducing the cost and time for the development of novel composite aircraft structures. It should be noted that the onset of failure in the above structures is still considered difficult to predict, due to composites displaying less noticeable failure indications. Thus, a failure criterion should be examined thoroughly for analysis. The criterion applied in the leading study is maximum strain failure, a noninteractive criterion that separately compares the respective lamina strain with the corresponding strength.

In this study, three different aspects were primarily explored. First, a linear static finite element analysis was conducted in Abaqus/standard [17] to validate the reliability of the approach in predicting the strength of a PRSEUS three-stringer panel with a multibay damage scenario subjected to a tensile load in accordance with Hashin failure criteria [18, 19]. The focus was placed on the load triggering the damage initiation in the panel, as it marks the beginning of material degradation and the reduction in the load-carrying capabilities in the structure. Data has been collected from experimental test [16], demonstrated in Figure 2, and is available to use as a reference to judge the adequacy of the finite element model. Second, a user-defined material (UMAT) [20] further implemented into Abaqus was employed to obtain more precise analysis results related to the experimental results. Third, the behavior of a repaired three-stringer damaged panel was analyzed to verify the application of UMAT at a relatively wider scale, as well as validate the role of the repair technique in restoring the load-carrying capabilities of the three-stringer panel.

2. Finite Element Model of Tension Stiffened Composite Three-Stringer PRSEUS Panel

Since finite element analysis (FEA) has been commonly applied as a primary analysis tool, the incorporation of features that will be computationally taxing should be excluded. It is noteworthy that the through-thickness stitches were not simulated on the grounds, so it had no effect on the analysis to any considerable degree as discussed in existing studies [16]. In addition, the metallic fasteners required to attach the repair panels were modelled alternatively. Furthermore, the metallic components were maintained in the elastic regime following airframe certification regulations [21].

2.1. Finite Element Model of Damaged Three-Stringer PRSEUS Panel. Assuming that the finite element modelling details are discussed in [6], it can be briefly mentioned that a dog-bone-shaped panel was modelled in Abaqus, a 1270 mm long three-stringer section of a PRSEUS panel; the pultruded rods were represented by two-node beam elements, and the composite panel's components were discretized with four-node shell elements, while solid elements were employed to discretize the foam core components (Figure 3). In general, the FE model had 91,999 shell elements and 788 beam elements. Since the composite components were modelled as elastic, Table 1 lists the stack orientation of the composite components, and Tables 2–4 present the material properties assumed for the analysis which were taken from the first phase report of the research conducted on the PRSEUS concept [6].

In the test performed in this study, metallic lugs were employed to uniformly distribute the in-plane displacement across the width of the panel at both ends. As a result, the BCs of the FE model were clamped at one end, whereas the out-of-plane displacements were constrained on the other end (Figure 4). A 152.4 by 6.35 mm opening was modelled to simulate a midbay damage scenario. It is noteworthy that the panel and damage configuration and dimensions are based on those adopted to investigate the panel's damage arrest capacities in [16].

Lastly, the FE model was subjected to a 100% design limit load (649,440.35 N) to define the load at which the damaged panel would demonstrate the initiation of failure. However, the damage propagation and damage arrest modes take on a critical significance in the study of the PRSEUS concept; they are not in the scope of this study.

2.2. Finite Element Model of Repaired Three-Stringer Panel. The repair concept was tested by Boeing Company and elucidated in [22]. The essential aim is to come up with a practical cost-friendly repair technique that would restore the load-carrying capabilities similar to or even better than those of a pristine PRSEUS panel. Thus, a Mohawk repair concept [23] is further explored in this study. This concept consists of two 2.54 mm thick upper repair pieces with a vertical portion parallel to the damaged stringer web, and the vertical portion rests on the surface of the stringer flange as it is displayed in Figure 5. Besides the 2.286 mm thick lower repair piece rests on the lower surface of the skin which can be seen in Figure 6, the repair pieces were made of an aluminum alloy and riveted together by titanium fasteners. However, to simplify the analysis, the fasteners were modelled with CONN3D2 connecter elements [17], and shell elements were employed in the discretization of the repair panels. In general, the entire assembly consisted of 18 fasteners connecting the two upper pieces together, 20 fasteners connecting the stringer web to the repair pieces, and 72 fasteners connecting the upper and lower repair pieces together and consequently to the panel. As mentioned above, the fasteners are modelled with connector elements and are highlighted in Figure 7. The locations and alignment of the fasteners were elucidated in [22], in which established design practices (e.g., those regarding spacing requirements between metallic fasteners applied to a

Figure 2: Damaged three-stringer PRSEUS panel being prepared for testing in Boeing Huntington Beach Test Lab [16].

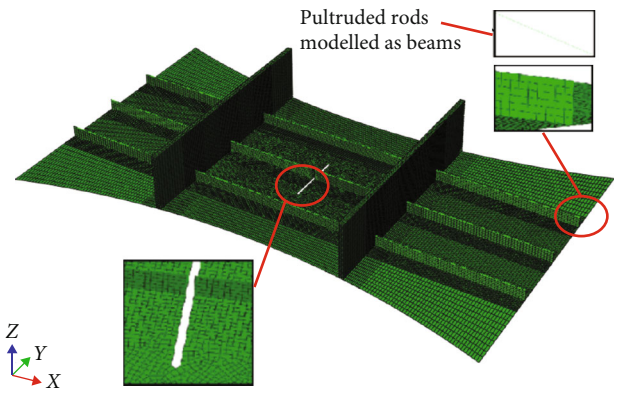

Figure 3: Damaged panel's mesh model.

Table 1: Three-stringer panel stack orientation.

Panel's component	Stack orientation with respect to the panel's length
Skin	(90)
Stringer	(0, 0)
Frame cap	(90, 90, 90)
Frame	(0, 0, foam, 0, 0)*

*0° (frame's length).

composite primary structure [24]) were explained. Only the repair panels were modelled as elastic-plastic in the analysis, and the panel was subsequently loaded till the ultimate load of 974,160.53 N.

Table 2: Material properties of noncomposite components [6].

Material	Foam core Rohacell 110WF	Rod toray T800/3900-2B	Aluminum alloy 7075-T6
E (MPa)	144.79	126,932.48	71,705.476
ν	0.32	0.3	0.33
ρ (t/mm^3)	$9.99e-11$	$1.60e-9$	$2.81e-9$
Tensile (yield) strength (MPa)	—	—	537.78 (475.74)

Table 3: AS4-VRM34 material properties (stack properties) [6].

Engineering constant	E_1 (MPa)	E_2 (MPa)	E_3 (MPa)	ν_{12}	ν_{13}	ν_{23}	G_{12} (MPa)	G_{13} (MPa)	G_{23} (MPa)	ρ (t/mm^3)
Numerical value	67,154.93	33,542.99	34,956.42	0.4	0.4	0.095	16,340.57	16,340.57	5515.81	$1.60e-9$

Table 4: Failure properties of stack components [6].

Longitudinal tensile strength (X^T)	Longitudinal compressive strength (X^C)	Transverse tensile strength (Y^T)	Transverse compressive strength (Y^C)	Longitudinal shear strength (S^L)	Transverse shear strength (S^T)
724.64	546.06	320.61	261.31	206.15	206.15

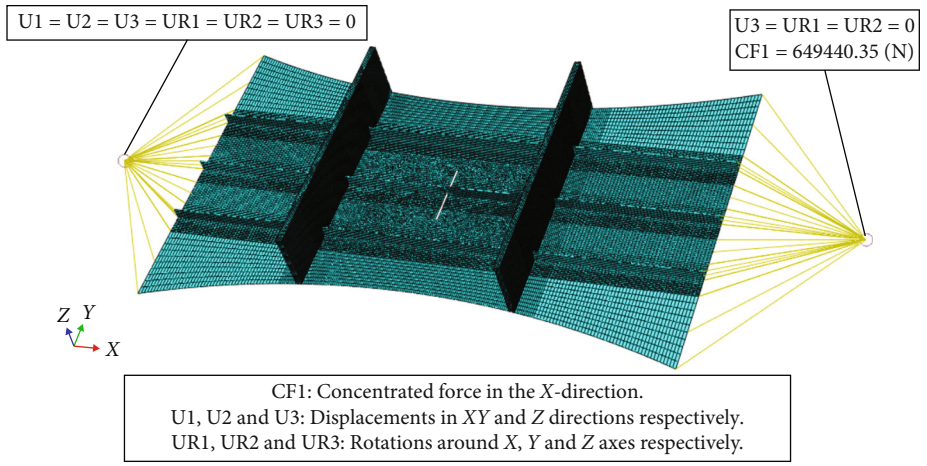

Figure 4: Damaged panel's boundary conditions.

3. Modified Hashin Failure and UMAT Implementation

When a composite with a high fiber volume fraction (e.g., carbon-epoxy composites) is subjected to tension, it is the fibers that carry the main portion of the load. In addition, fiber tensile failure releases large energy that might trigger fibers or matrix in the vicinity to fail and evidently may cause catastrophic failure if the load distribution in a structure is not adequate. With this in mind, a failure criterion that can distinguish between different matrix and fiber modes was prioritized, namely, Hashin failure criteria, to predict the onset of damage in the linearly elastic material. It should also be pointed out that Hashin criteria are advantageous in the damage analysis of geometrically compacted composite structures [25].

3.1. Introduction of Hashin Failure Criteria. Hashin failure criteria are interactive criteria [26] that have been considerably popular in composite structural applications for their ease of use. Moreover, it attributes the failure of a structure to two different physical mechanisms, fiber-dominated failures, and matrix-dominated failures. They consider the possible interactions of stresses or strains acting on a lamina, while simultaneously distinguishing between the characteristics of fiber breaking in tension or compression and matrix

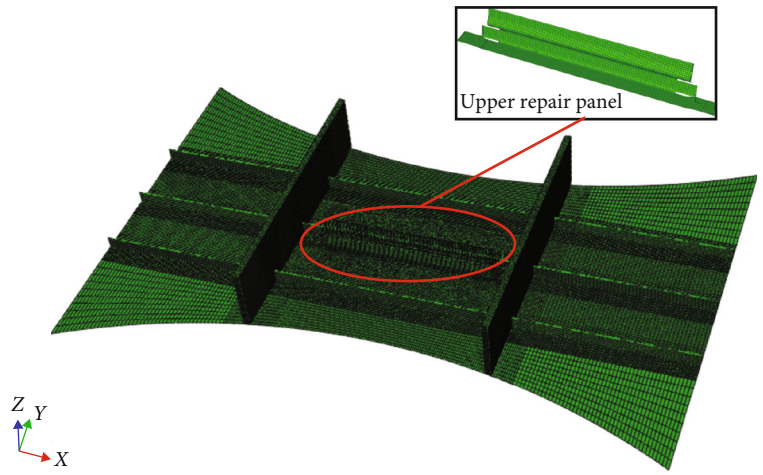

Figure 5: Repaired panel's mesh model (upper view).

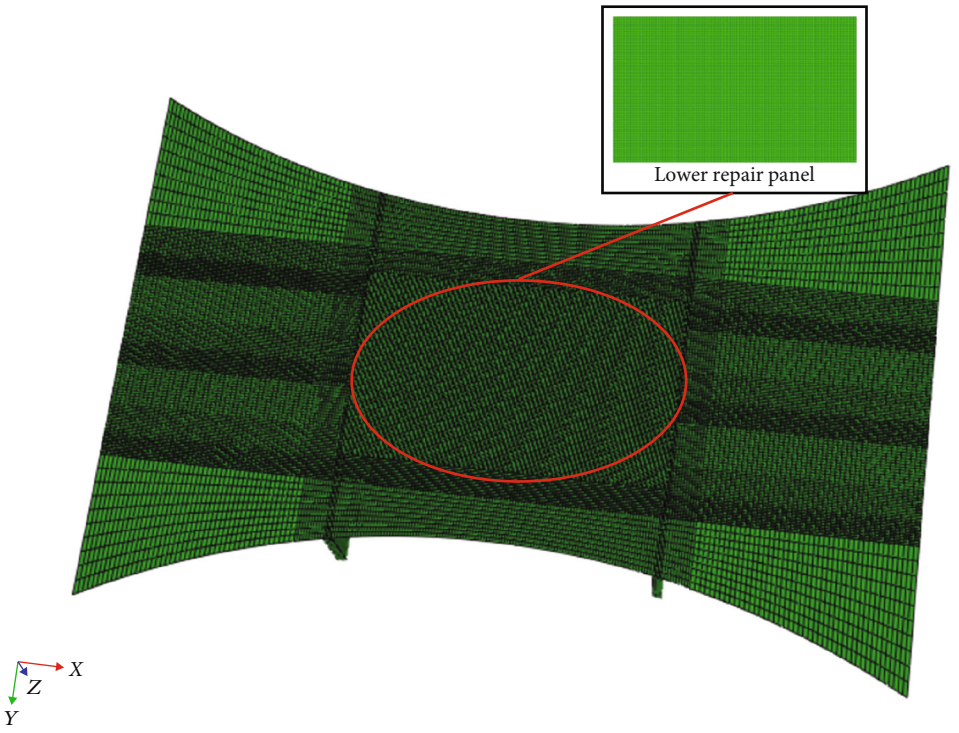

Figure 6: Repaired panel's mesh model (lower view).

breaking in tension or compression. Hashin failure criteria were initially developed for the research on unidirectional composites and gradually broadened to cover a wide variety of forms of multidirectional laminates.

Abaqus software implements Hashin failure theory and predicts the damage initiation in the four different damage initiation mechanisms in accordance with the general forms.

Fiber tension ($\sigma_{11} \geq 0$):

$$F_{\mathrm{ft}} = \left(\frac{\sigma_{11}}{X^{\mathrm{T}}}\right)^2 + \alpha\left(\frac{\sigma_{12}}{S^{\mathrm{L}}}\right)^2 = 1. \quad (1)$$

Fiber compression ($\sigma_{11} < 0$):

$$F_{\mathrm{fc}} = \left(\frac{\sigma_{11}}{X^{\mathrm{C}}}\right)^2 = 1. \quad (2)$$

Matrix tension ($\sigma_{22} \geq 0$):

$$F_{\mathrm{mt}} = \left(\frac{\sigma_{22}}{Y^{\mathrm{T}}}\right)^2 + \left(\frac{\sigma_{12}}{S^{\mathrm{L}}}\right)^2 = 1. \quad (3)$$

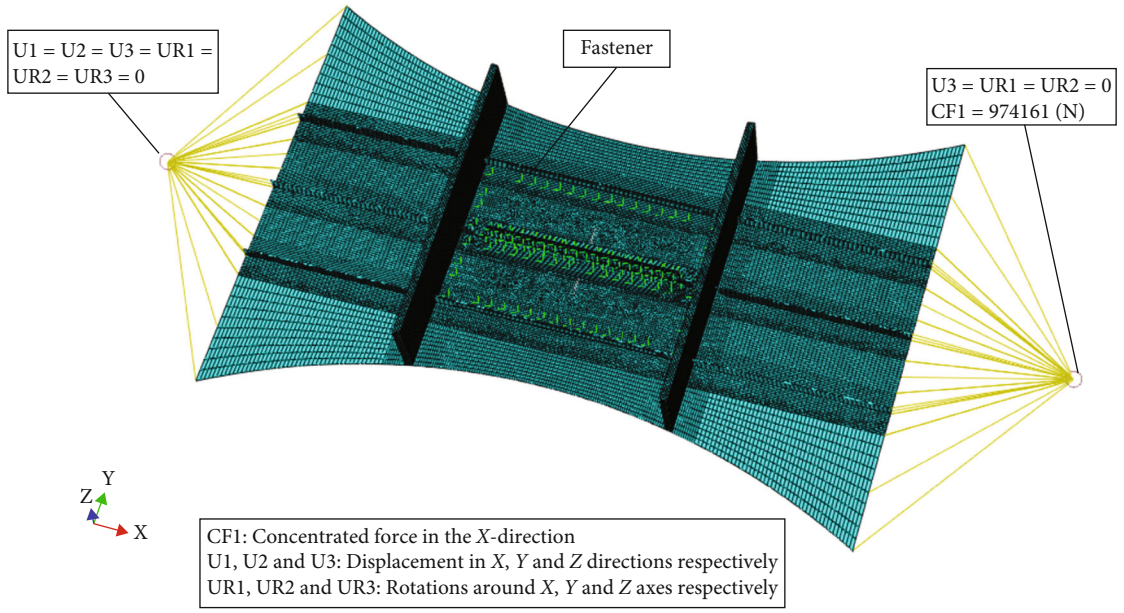

Figure 7: Repaired panel's boundary conditions and fastener locations.

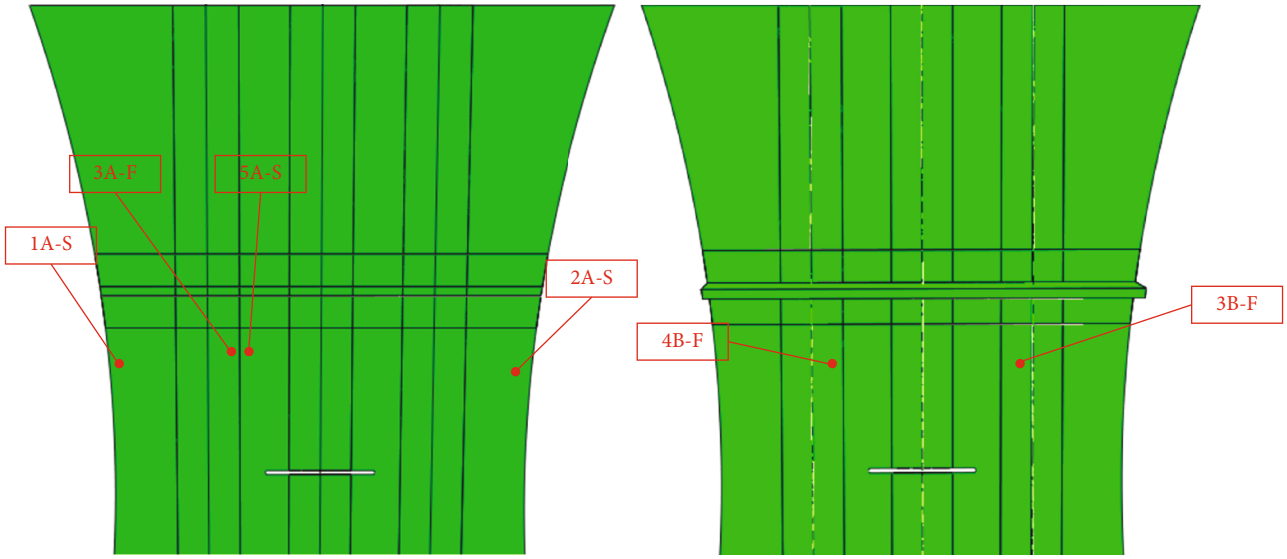

Figure 8: Locations of the simulated strain gages.

Matrix compression ($\sigma_{22} < 0$):

$$F_{mc} = \left(\frac{\sigma_{22}}{2S^T}\right)^2 + \left[\left(\frac{Y^C}{2S^T}\right)^2 - 1\right]\frac{\sigma_{22}}{Y^C} + \left(\frac{\sigma_{12}}{S^L}\right)^2 = 1, \quad (4)$$

where σ_{ij} are stress components; X^T and X^C denote tensile and compressive strengths in the fiber direction, respectively; Y^T and Y^C represent tensile and compressive strengths in the matrix direction, respectively; and longitudinal and transverse shear strengths are denoted by S^L and S^T, respectively. Besides, α is a coefficient that signifies the contribution of the shear stress to fiber tensile failure initiation.

3.2. UMAT Implementation of Modified Hashin Failure Criteria. Abaqus adopts an iterative approach by first estimating the strain increment $\Delta\varepsilon$ depending on boundary conditions and the total time increment, after which the material model is adopted to calculate the stresses and the Jacobian before it solves the balance equation. If the solution is converged, it will pass through the next increment.

UMAT replaces the material model, which explains why it should provide a definition of material properties and

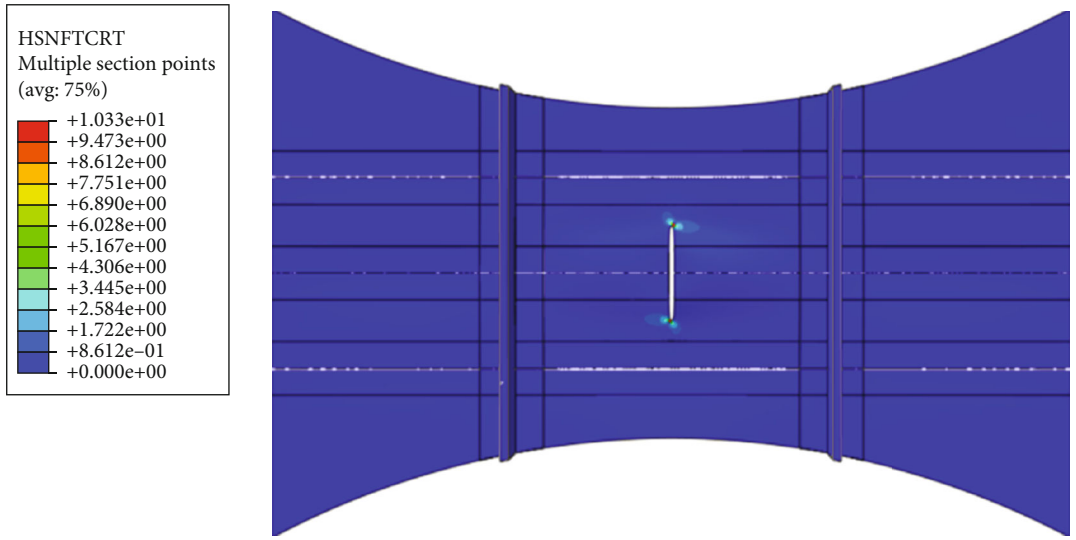

Figure 9: Fiber tensile damage initiation in the standard analysis.

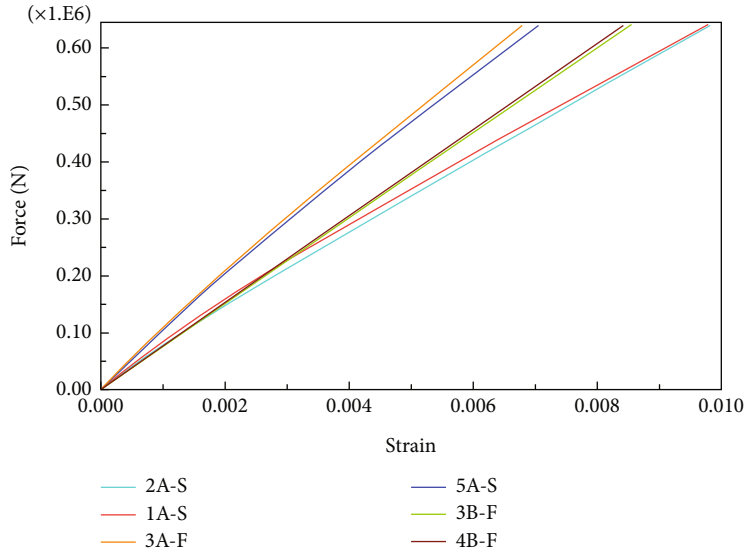

Figure 10: Standard analysis load-strain progression.

current strain increment and calculate current stresses based on the constitutive relations. In the three-dimensional analysis of a linear elastic orthotropic material, the stress-strain relation is expressed below:

$$\{\sigma\} = \begin{Bmatrix} \sigma_{11} \\ \sigma_{22} \\ \sigma_{33} \\ \sigma_{12} \\ \sigma_{13} \\ \sigma_{23} \end{Bmatrix} = \begin{bmatrix} C_{11} & C_{12} & C_{13} & 0 & 0 & 0 \\ C_{12} & C_{22} & C_{23} & 0 & 0 & 0 \\ C_{13} & C_{23} & C_{33} & 0 & 0 & 0 \\ 0 & 0 & 0 & C_{44} & 0 & 0 \\ 0 & 0 & 0 & 0 & C_{55} & 0 \\ 0 & 0 & 0 & 0 & 0 & C_{66} \end{bmatrix} \begin{Bmatrix} \varepsilon_{11} \\ \varepsilon_{22} \\ \varepsilon_{33} \\ \gamma_{23} \\ \gamma_{31} \\ \gamma_{12} \end{Bmatrix} = [C]\{\varepsilon\}, \tag{5}$$

where the stiffness coefficients $C_{i,j}\,(i, j = 1, \cdots, 6)$ are defined for elastic material constants. Besides, the current stress is calculated by the following equation:

$$\sigma_{ij} = \sigma_{ij} + C_{ji} * \varepsilon_{ij}\,(j \le i). \tag{6}$$

Subsequently, the stresses are adopted to evaluate the state of fiber and matrix damage by substituting the values in the corresponding Hashin equations (1)–(4), and thus, damage is initiated when the quadratic nominals reach the value 1.

The transverse shear stiffness must be defined when UMAT is employed to define a material that employs shell elements, and since this study is conducted on a linear elastic orthotropic

Table 5: Comparison between standard analysis and UMAT analysis in values of axial displacement and maximum in-plane strain in composite components at damage initiation.

Composite component	Axial displacement U1 (mm)		Maximum in-plane strain	
	Standard analysis	UMAT analysis	Standard analysis	UMAT analysis
Skin	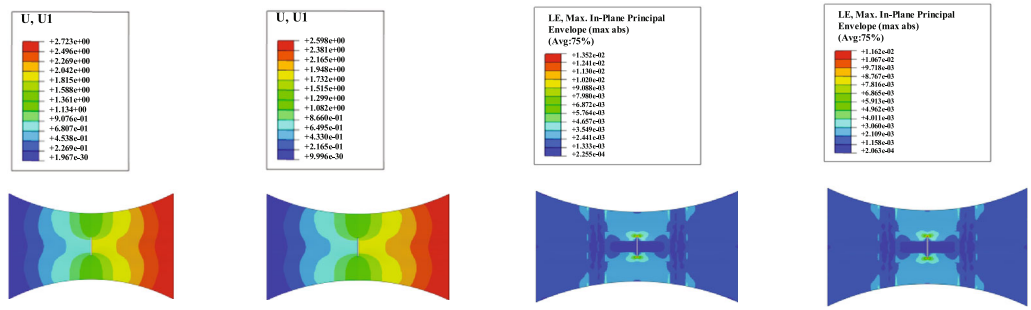			
Stringer strap	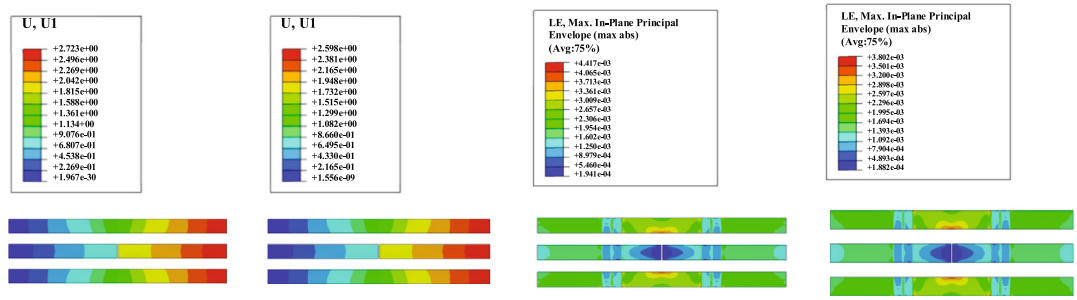			
Stringer flange	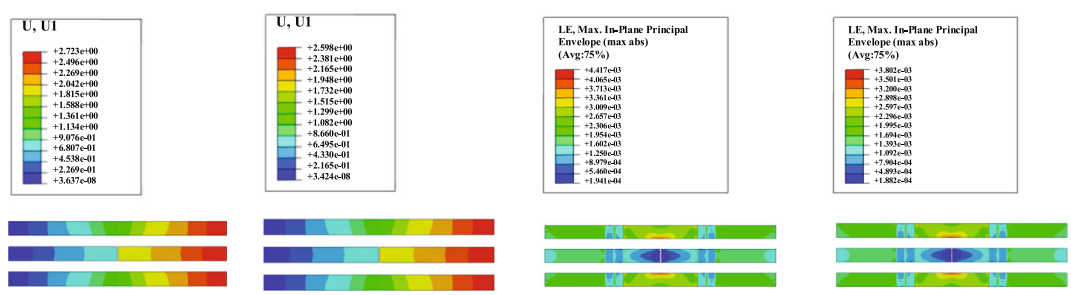			
Frame strap	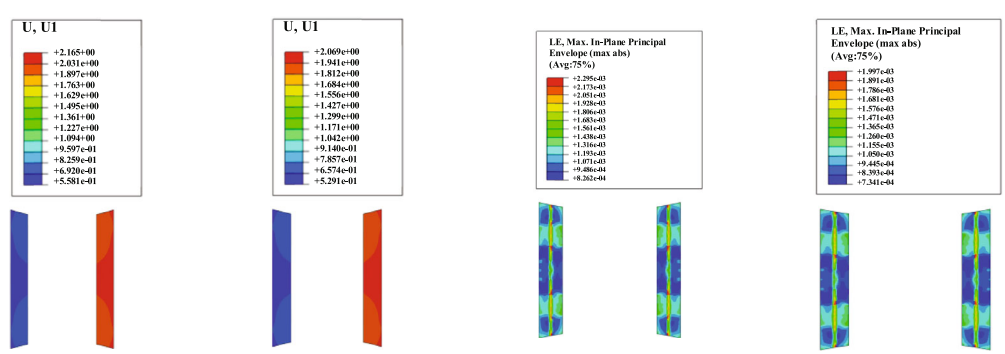			

Table 5: Continued.

Composite component	Axial displacement U1 (mm)		Maximum in-plane strain	
	Standard analysis	UMAT analysis	Standard analysis	UMAT analysis
Frame flange	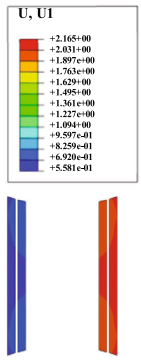	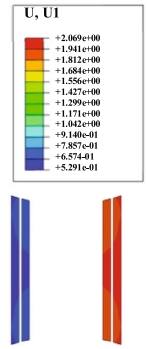	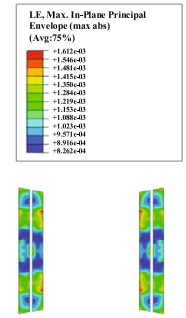	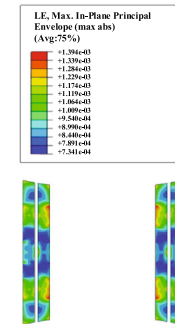
Stringer web	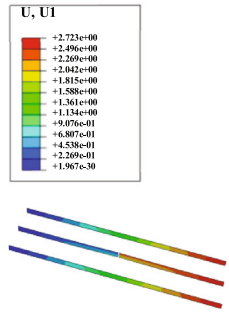	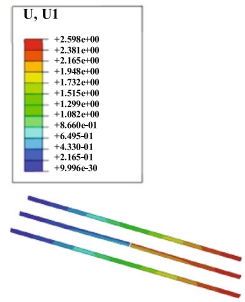	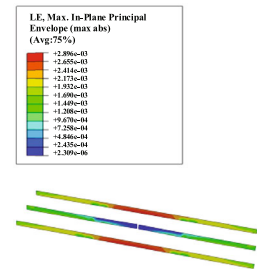	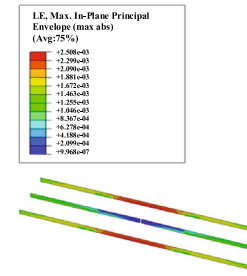
Frame	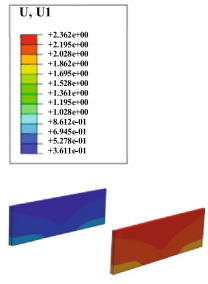	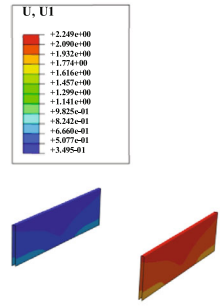	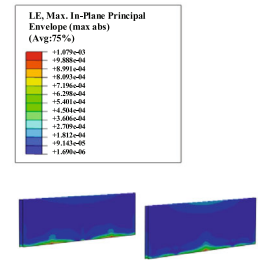	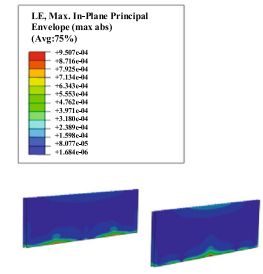

material, the transverse shear stiffness is defined as

$$K_{11}^{ts} = \frac{5}{6} G_{13} t,$$
$$K_{22}^{ts} = \frac{5}{6} G_{23} t, \quad (7)$$
$$K_{12}^{ts} = 0,$$

where 5/6 denotes the shear correction factor, G_{13} and G_{23} represent the shear moduli in the out-of-plane direction, and t is the shell's thickness.

4. Failure Analysis of Damaged Three-Stringer PRSEUS Panel

It should be stressed out once again that the panel's behavior after damage initiation is of no interest to this study. As previously mentioned, the material exhibits linear elastic progressive behavior. Since there are no critical load instances in the scope of this study, the time period of the analysis can be selected arbitrarily. Strain's change with respect to force was monitored in six different locations, as illustrated in Figure 8. The above locations were selected to simulate the strain gage locations from the experiment in Ref. [16].

4.1. Failure Analysis of Damaged Three-Stringer PRSEUS Panel Based on Hashin Failure Criteria. The load was distributed linearly throughout the total time increment. As depicted in Figure 9, the stress then accumulated mainly around the tips of the damage location, so the tips exceeded the yielding stress when the panel was loaded at 200,315 N, and the failure was then initiated. However, the elastic-plastic material behavior was not triggered since it was not in the scope of the analysis.

As depicted in Figure 10, the locations 1A-S and 2A-S showed a distinctly quicker progression of strain with respect to load, revealing that the panel was transmitted from 4 stacks in the frame cap to a single skin stack in the above regions, and the percentage of fibers positioned in

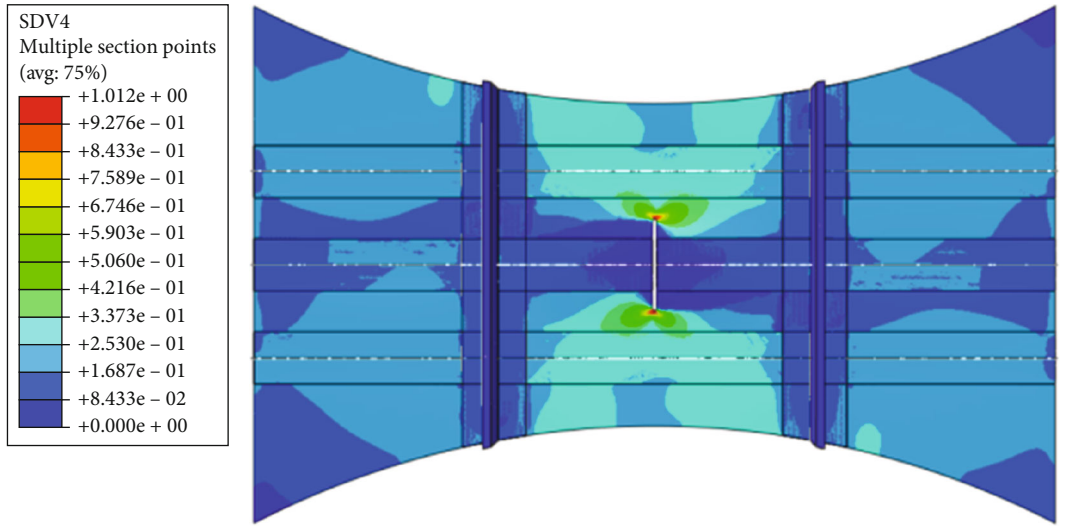

Figure 11: Fiber tensile damage initiation in the UMAT analysis.

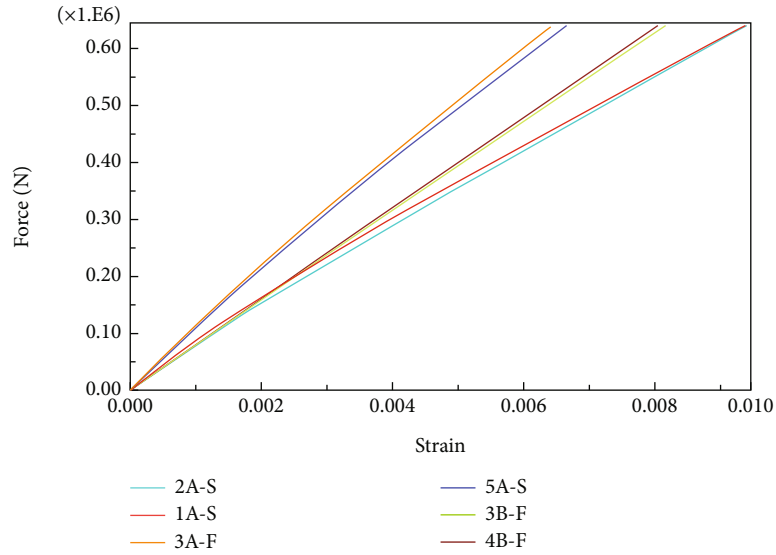

Figure 12: UMAT analysis load-strain progression.

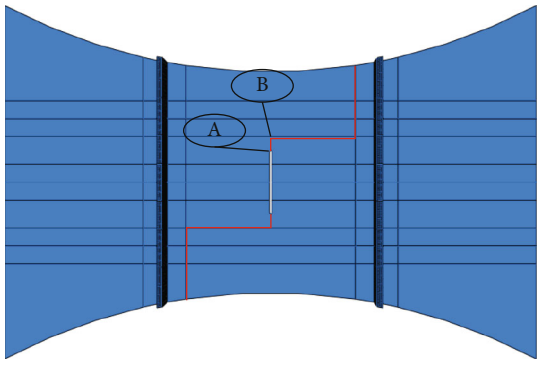

Figure 13: The path of damage propagation in the three-stringer panel that was obtained from experimental data [16].

the axial direction was low. Although 3A-F and 5A-S were placed in the vicinity of discontinuities, the strain progressed still in a relatively slower manner due to the two side stringer regions having a relatively higher stiffness since a large portion of the fiber was in the axial direction. Notably, some curves overlapped since there was an identical response of strain in some of the chosen locations. The effect of stress concentration around the tips of the notch could further be examined from the results of the maximum in-plane strain depicted in Table 5, thus revealing that the middle stringer location had a lower value of in-plane strain at the vicinity of the damage compared with the outer two stringer locations in all the components of the panel.

4.2. Failure Analysis of Damaged Three-Stringer PRSEUS Panel Based on Modified Hashin Failure Criteria. Different values of the coefficient α were considered till finally settling on a value of 0.75.

The solution-dependent state variable SDV4 represents the Hashin tensile damage initiation criterion; the location of the damage initiation in Figure 11 was not debatable.

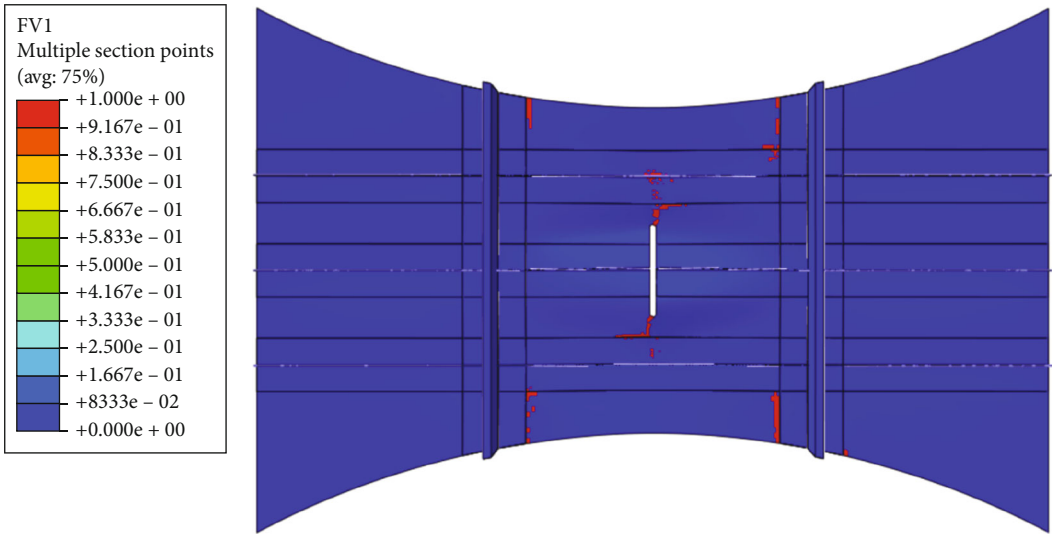

Figure 14: Evolution of tensile fiber damage in three-stringer panel using Hashin failure criteria, implemented through USDFLD subroutine.

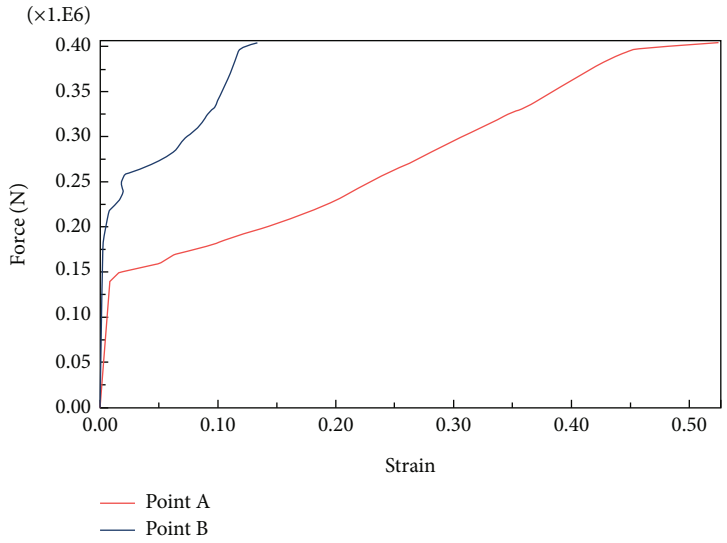

Figure 15: Force-strain diagram in locations A and B.

Table 6: Comparison of strain-load results in the simulated gages.

Strain gage	Test value [16]	Standard analysis	Margin of error (%)	UMAT analysis	Margin of error (%)
1A-S	0.0024	0.0026	8.33	0.0025	4.16
2A-S	0.0026	0.0028	7.69	0.0027	3.84
3A-F	0.00175	0.0019	8.57	0.0018	2.85
3B-F	0.0026	0.0027	3.84	0.00257	1.15
4B-F	0.0026	0.0025	3.84	0.0025	3.84
5A-S	0.0018	0.00192	6.66	0.00184	2.22

However, the load at which the failure was initiated uses a user material subroutine equal to 204,815 N; it was relatively larger due to a change in the stiffness properties provided by UMAT, as well as the change in shear stress contribution.

When examining Figure 12 and the strain values in Table 5, it was found that in most locations, the strain increased at a slightly slower rate, and in correspondence with the previous segment, the stress concentration effects were clearly distinguishable in the panel behavior which displayed lower strain in its middle section along the middle stringer position, whereas the outer stringers showed localized higher values considering their proximity of the tips of the notch.

Unlike the standard analysis, it was revealed that location 3B-F briefly displayed a quicker response to load by having the highest strain value amongst the monitored locations before the locations 1A-S and 2A-S eventually progressed faster, probably because it was around the web where the panel had a geometrical discontinuity.

4.3. Nonlinear Analysis of Damage Progress in Three-Stringer PRSEUS Panel Based on Modified Hashin Failure Criteria.

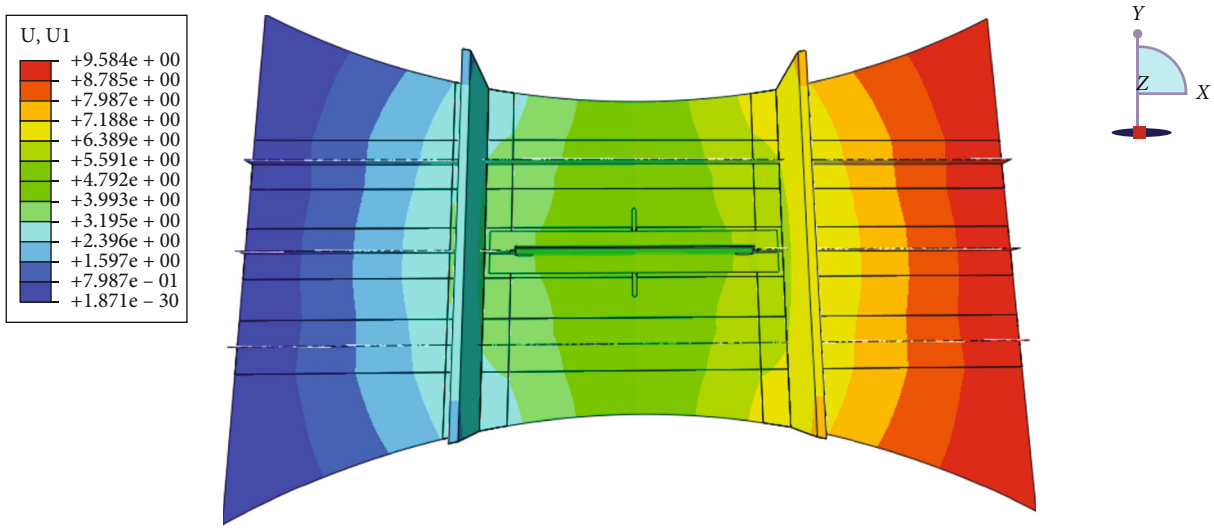

Figure 16: Standard analysis repaired panel in-plane displacement (mm).

Once the damage is initiated, the strength of the material will be primarily impacted by failure propagation, and it will eventually give rise to a nonlinear behavior [27–30]. According to the variables of damage, rules of behavior are used to describe the reduction of the modulus of stiffness. The ability to accurately anticipate the progressive damage of the three-stinger panel could not be completely explored due to the inaccessibility of several material properties, including fracture energy values. However, a different approach was employed to check and confirm the path of failure evolution which is demonstrated in Figure 13 by using the user subroutine USDFLD and Hashin failure criteria.

This approach is quite conservative since it predicts a weaker structure than the experiment has shown by instantly reducing to zero the stiffness of the components that meet the requirements for damage initiation. Although the USDFLD subroutine, unlike the UMAT subroutine, does not allow for the comprehensive definition of new mechanical behavior for a material, it is nevertheless practical to assign material attributes depending on variables that are more important to the study. It requires considerably less understanding of continuum mechanics, which makes it easier to write and takes less time to simulate a material behavior.

It can be seen in Figure 14 that when the damage reached the stringer, it was indeed stopped and rotated, but a little amount of it continued to go forward directly from point B, and early damage was started by the frame cap where geometric discontinuities exist. As stated earlier, the value which denotes the in-plane shear's contribution was set at 0.75 in light of the significant improvement in analysis accuracy noted in the damage initiation study's earlier part. The force-strain relationship in the locations that represent point A and point B is represented in Figure 15. And it can be seen that the damage expanded to the outside stringers when the applied stress reached around 238,264 N.

4.4. Experimental Verification of Analysis Results. As depicted in Table 5, all the composite components tended to have slightly smaller axial displacement values at the onset of failure when a user material model was implemented. Likewise, the maximum in-plane strain values were noticeably smaller for all the components.

The test conducted at NASA Langley Research Center [16] suggested that the damage initiation started when the distributed load was equal to 204,618.19 N, implicating that the Abaqus implemented Hashin criteria showed a 2.10% smaller value, underestimating the strength of the panel to a negligible degree, while the user material subroutine achieved a 0.11% larger value.

Furthermore, the strain progression with respect to load was compared to the experimental results [16], and the results are listed in Table 6. In 4 out of 6 locations, the behavior of the panel was remarkably improved, notably in the skin's lower section and the flange's upper section; the two analyses were different from each other by up to 5.72% with the UMAT model proven to be more adequate in predicting more precise behavior.

In the nonlinear analysis of damage progression in the structure, the damage at point A was recorded at a substantially early section of load application; it suggested that the load approximately equals 159,428 N, making this value 22.08% smaller than the experimental value. On the other hand, the load subjected to the panel at the point when the damage reaches point B in the structure equals 238,264 N, and this is 16.30% smaller than the value obtained experimentally which equals 284,686.18. The path is consistent with the characteristics concerning damage arrest offered by the PRSEUS structures.

5. Failure Analysis of Repaired Three-Stringer Panel

The primary purpose of a repair concept refers to the restoration of capacities the same as or slightly better than those conveyed by a pristine panel.

5.1. Failure Analysis of Repaired Three-Stringer PRSEUS Panel Based on Hashin Failure Criteria. The panel revealed

Table 7: Comparison between standard analysis and UMAT analysis in values of axial displacement and maximum in-plane strain in composite components at end of the load application.

Composite component	Axial displacement U1 (mm)		Maximum in-plane strain	
	Standard analysis	UMAT analysis	Standard analysis	UMAT analysis
Skin	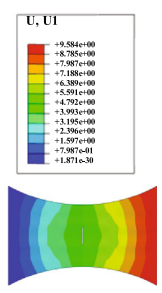	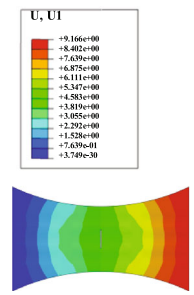	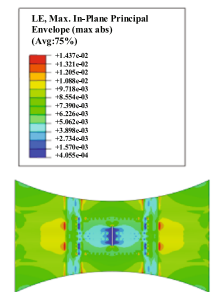	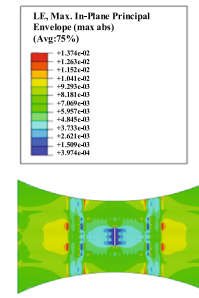
Stringer strap	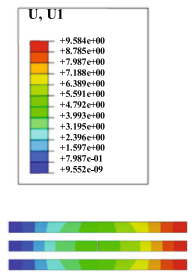	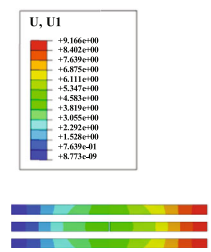	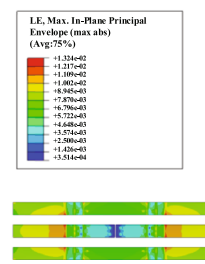	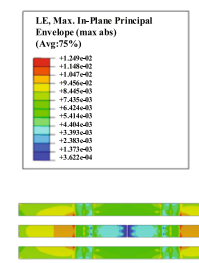
Stringer flange	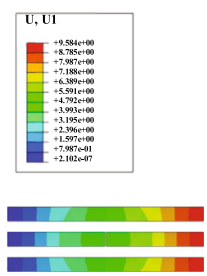	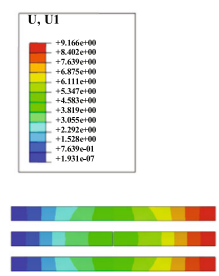	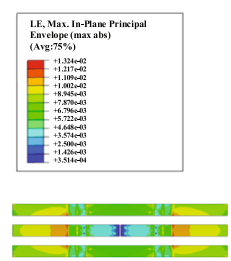	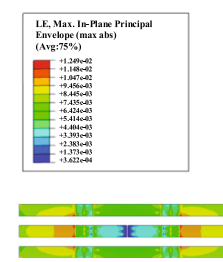
Frame strap	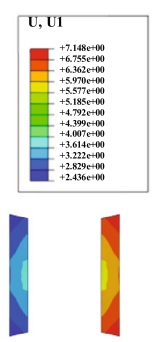	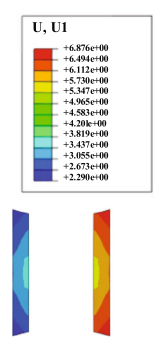	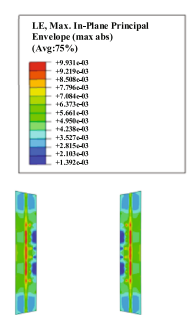	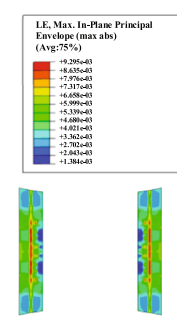
Frame flange	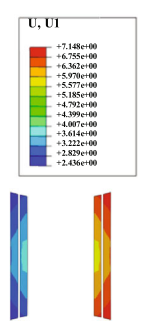	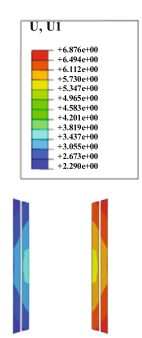	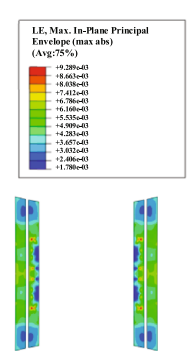	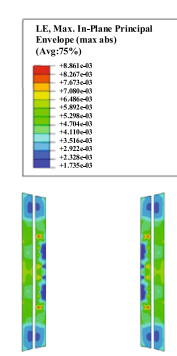

Table 7: Continued.

Composite component	Axial displacement U1 (mm)		Maximum in-plane strain	
	Standard analysis	UMAT analysis	Standard analysis	UMAT analysis
Stringer web	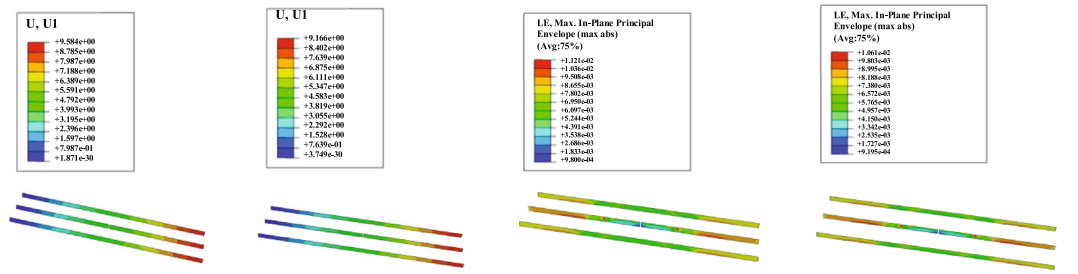			
Frame	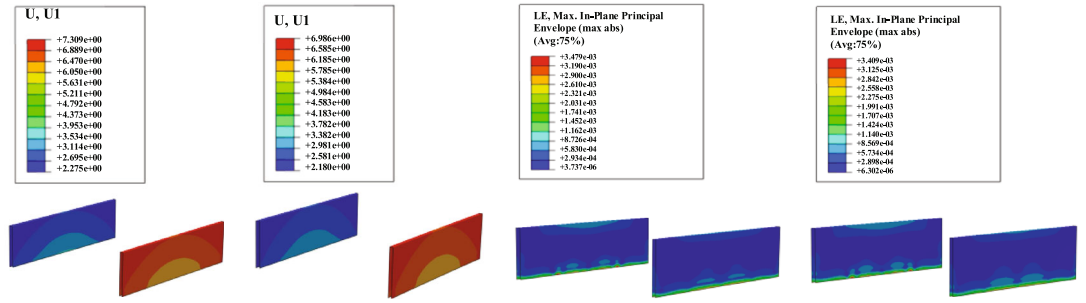			

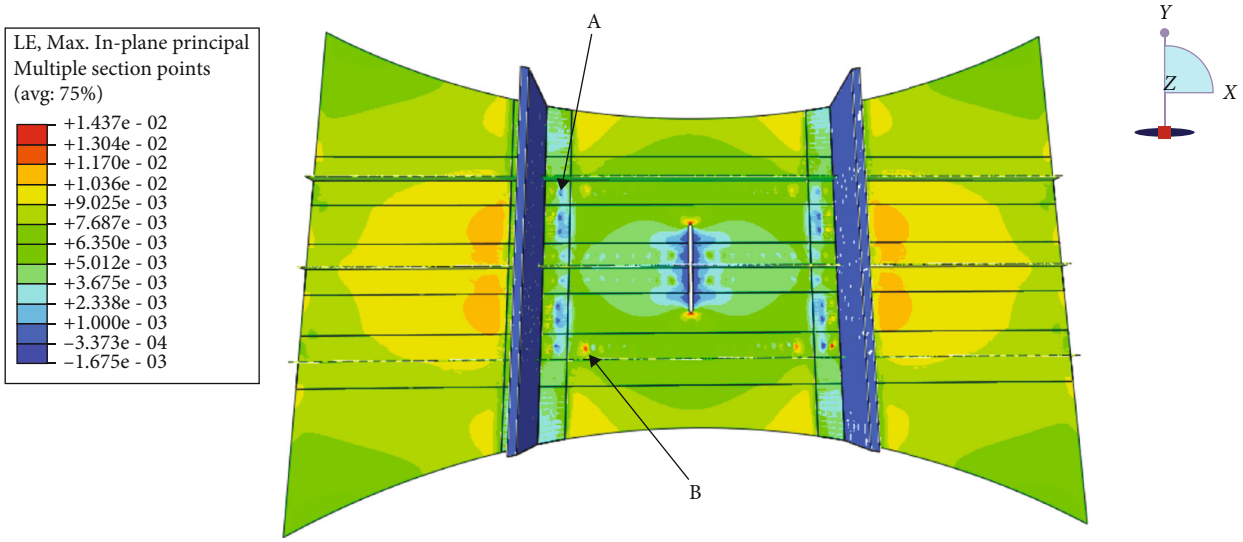

Figure 17: Standard analysis repaired panel maximum in-plane principal strain (the repair panel is removed).

the start of failure at a load approximately 30% larger than the ultimate load, while Figure 16 depicts that the axial displacement corresponding to the ultimate tensile load was 9.584 mm, 4.96% smaller than the axial displacement of the pristine panel. It also illustrates a moderately uniform in-plane displacement distribution across the width of the panel assembly. Table 7 presents a less uniform distribution across the frame cap components. As depicted in Figure 17, the onset of failure occurred in the locations of the four fastener joints, denoted by A at the corners that were supposed to connect the lower repair panel to the skin and frame stacks. Although the panel consisted of stacks in the above vicinities, most of the stacks were positioned in the transverse direction. Further examination of Table 7 revealed that the allowable maximum strain value of 0.0105 mm/mm was exceeded in small areas in the vicinity of frame flange edges and in the outer fastening joints on the web component.

The above regions had discontinuities where the single-stack skin component was transited to the frame cap section comprising six stacks. The ultimate strain was also exceeded in the same locations where the initiation of damage occurred as well as the tips of the damage location. Consequently, the prime reason for the high ultimate strain values was the discontinuities.

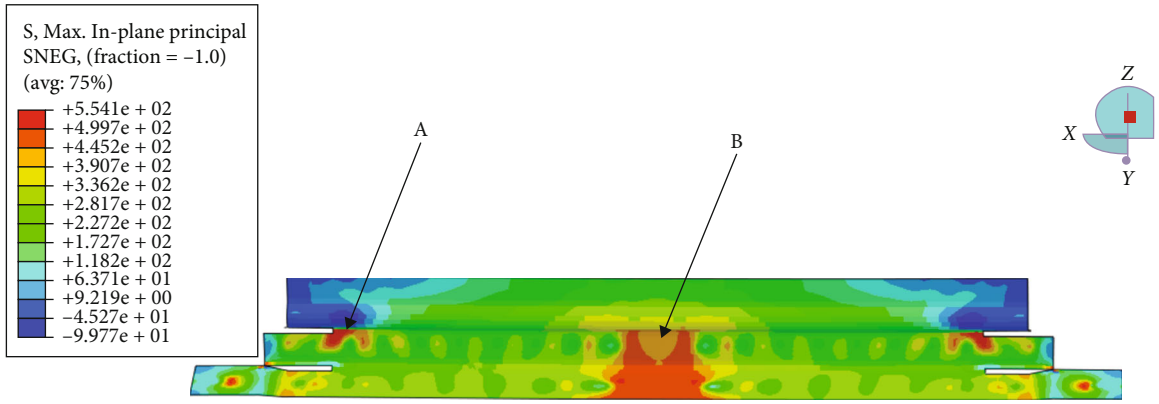

Figure 18: Standard analysis maximum in-plain principal stress in the upper repair panel (MPa).

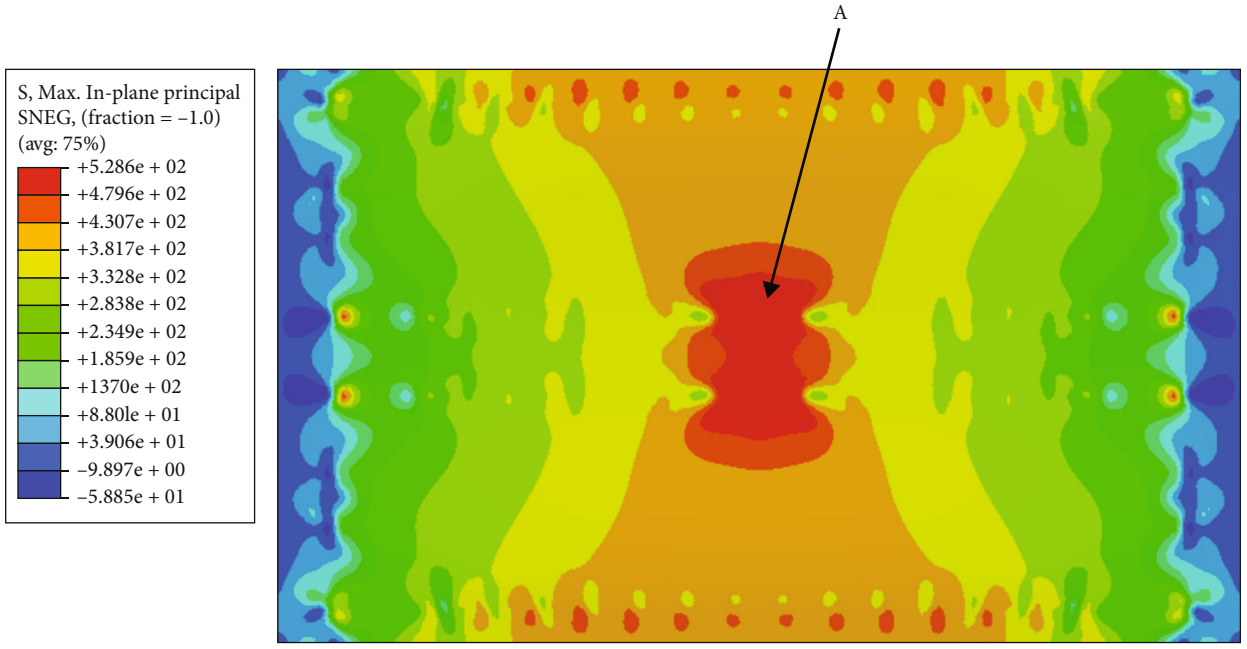

Figure 19: Standard analysis maximum in-plain principal stress in the lower repair panel (MPa).

Figures 18 and 19 illustrate the maximum principal stress distribution in the upper repair panel and lower repair panel, respectively, suggesting that the repair panels did not exceed the limit stress of 475.738 N/mm^2 when the load applied on the panel corresponding to the limit load; however, when it corresponded to the ultimate load, the yielding stress was exceeded in the upper repair panel in the midspan region around the location of the damage as well as in the location of the fastener at the outmost end of the repair panel. Besides, the ultimate stress value of 537.791 N/mm^2 was exceeded in the location denoted by A due to stress concentration where the panel changed geometry. In the lower repair panel, the ultimate load was not exceeded, whereas the regions at the proximity of the damage exceeded the yielding stress allowing for a plastic response regime.

5.2. Failure Analysis of Repaired Three-Stringer PRSEUS Panel Based on Modified Hashin Failure Criteria. The user-defined material denotes the initiation of failure at a load roughly 12% smaller than the limit load. When the ultimate load value was reached, the axial displacement corresponded to 9.166 mm as illustrated in Figure 20, a value smaller than the one obtained by the standard Abaqus analysis and 9.10% smaller than the pristine panel axial displacement at the equivalent load.

Although the in-plane distribution was overall similar to the previous analysis, with the displacement in the left frame being larger in the vicinity of the middle stringer and smaller in the vicinity of the two outer stringers and the right frames displaying a displacement smaller in the vicinity of the middle stringer and larger in the outer two stringers due to the middle stringer having a relatively higher stiffness. However, the user material subroutine analysis revealed that the change in the displacement distribution was sharper. Figures 21 and 22 depict the same localization of stress in the repair panels as the one demonstrated in the standard analysis. The above localized behaviors were visible in the analyzed panel where the largest strain values are noted in

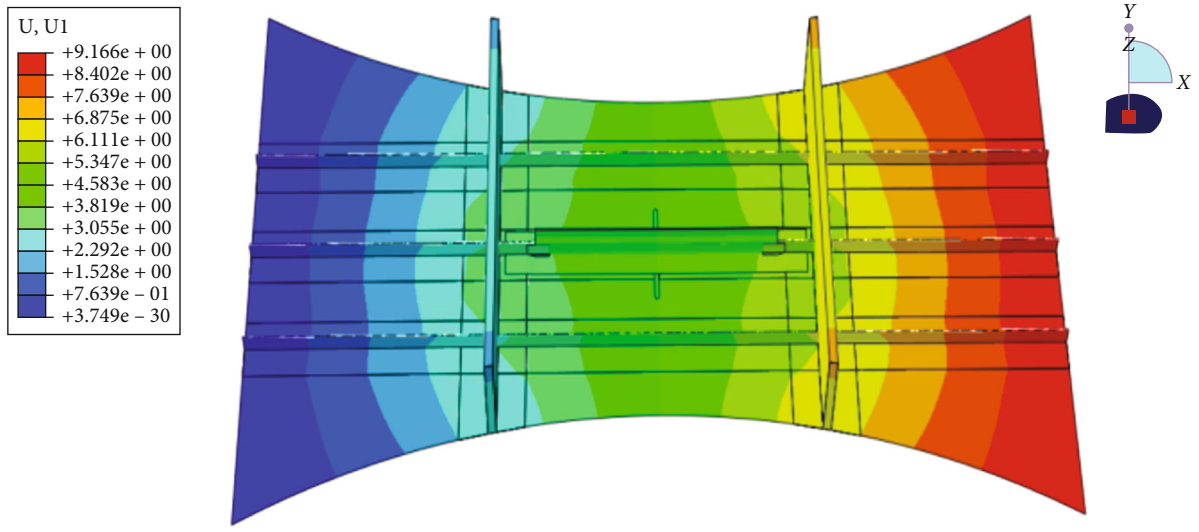

Figure 20: UMAT analysis repaired panel in-plane displacement (mm).

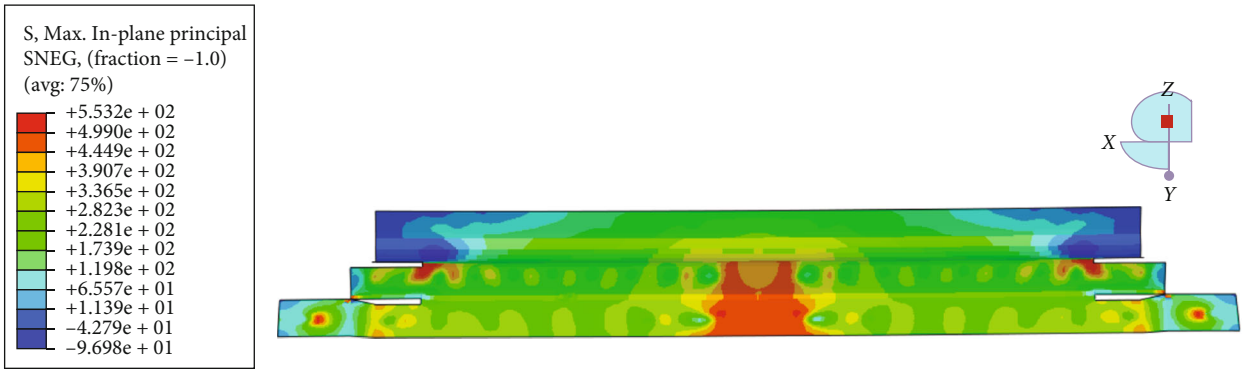

Figure 21: UMAT analysis maximum in-plain principal stress in the upper repair panel (MPa).

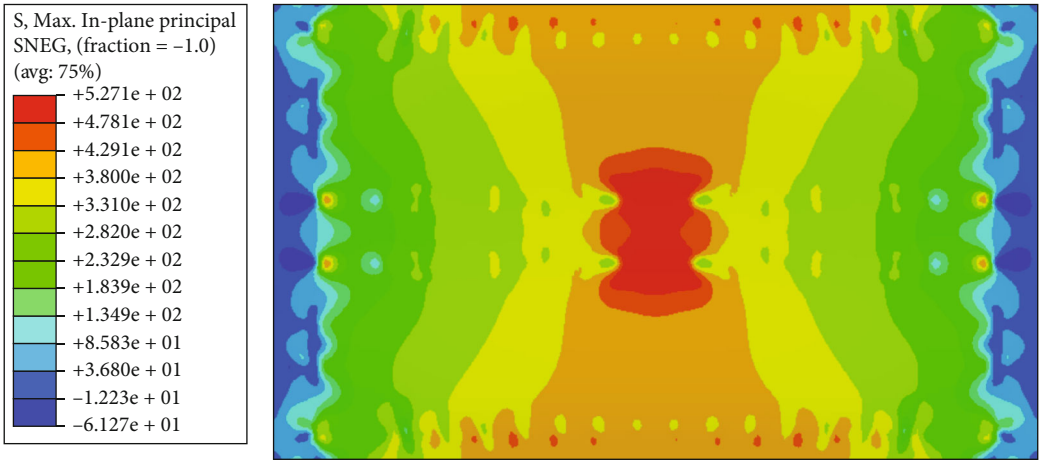

Figure 22: UMAT analysis maximum in-plain principal stress in the lower repair panel (MPa).

Figure 23 by A, B, and C, in regions on the web at the vicinity of the outer fastener, as well as the corner fastener connecting the lower repair panel with the panel. The above region had a larger percentage of fiber positioned parallel to the y-axis.

5.3. Experimental Verification of Analysis Results. Assuming that an insignificantly smaller amount of load was carried by the test panel instead of the repair panels, it was found that the maximum principal stress was also distributed over the upper and lower repair panels though a slight 0.16% reduction

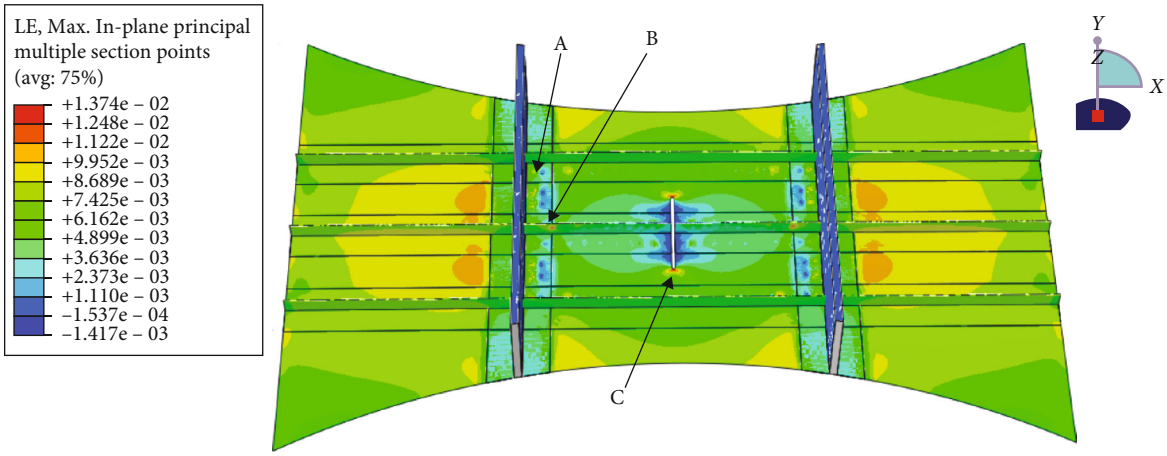

Figure 23: UMAT analysis repaired panel maximum in-plane principal strain (the repair panels are removed).

in the maximum value found for the upper repair panel and 0.28% for the lower panel in the UMAT analysis. Although a plastic response was triggered in small areas, no significant geometric nonlinearities were found in the analyses, and the response was correlated with the previous work [31].

Similar to the damaged panel's analyses, the axial displacement and the maximum in-plane strain values were considerably smaller in the UMAT analysis in all the composite components, as shown in Table 7.

As revealed by the available test results, a repaired panel had an axial end displacement of 9.1694 mm under the ultimate tensile load. Although the Abaqus implemented analysis and the UMAT implemented analysis indicated the values smaller than the pristine panel axial displacement, a 4.52% larger value for the first and 0.03% smaller value for the latter were obtained. However, the comparison of the in-plane displacement demonstrated the panels to be stiffer than the pristine panel. Moreover, the early initiation in the second analysis led to a questionable conclusion that should be investigated in future studies.

6. Conclusion

A model of a damaged three-stringer PRSEUS panel was investigated in accordance with Hashin failure criteria to verify the reliability of the above criteria in predicting the initiation of damage when implemented in a standard analysis or in using the user material subroutine in the Abaqus software, while extending the analysis to further investigate the behavior of a repaired panel. Thus, the following conclusion was drawn:

(i) Under tensile load, Hashin failure criteria were adopted to make predictions correlated with the experimental results obtained from the report [16], which calculated values of strain with a margin of error between 3.84% and approximately 8.57%. In addition, the 2.10% margin of error in predicting the load corresponding to the onset of failure developed confidence in the simplified approach of the analysis and the convenience of utilizing Hashin failure criteria. They already are built-in Abaqus software and considerably easy to use taking that strength data is available. Moreover, Hashin criteria comply with the use of shell elements, allowing for a significantly less computation time and power. Furthermore, the FEM approach demonstrated a logical distribution of strain in the different components of the structures, where higher values were displayed in locations around geometrical discontinuities, locations in the vicinity of the damage, or locations with low fiber portion oriented in the X-direction

(ii) The user material subroutine was demonstrated to have a considerable effect on giving a more precise and realistic prediction of the onset of failure by calculating more precise values of strain for the damaged panel analysis. It yielded in considerably reducing the margin of error of the above strain values from the mentioned domain to values from 1.15% to 4.16%. This precision was further demonstrated in the analysis of the repaired panel, notably in the value of the axial displacement, which was indicated to have a value 4.5% larger than the experimental value using the built-in model and 0.03% smaller than the experimental when implementing the failure model through UMAT. In addition, the lower values of strain distribution in the components for the higher value of damage initiation load indicate that the stiffness of the panel is preserved, which further developed confidence in the modified Hashin failure criteria implemented based on the user-defined material model

(iii) Implementing Hashin failure criteria through the USDFLD subroutine provided an approximate idea of damage propagation in a three-stringer PRSEUS panel regardless of the lack of experimentally obtained parameters. These parameters are still important in accurately analyzing the response of

the panel to axial load, as it is seen that the integrity of the structure is substantially underestimated, as this subroutine predicted the onset of failure at a value of load 22.08% smaller than the experimental data, in addition to predicting damage to reach the stringers when the load was 16.30% smaller than expected

(iv) The Mohawk repair technique could be of great value when designed properly, prompting a panel as stiff as the pristine design. The approach of using CONN3D2 connector elements saves effort and time in modelling fasteners, and it demonstrates some seasonably reliable analysis results. The alignment of fasteners and the distance between them could significantly affect the ultimate tensile strength of the panel in form of localized behavior in regions of discontinuities

The results of this study assert great confidence to further apply the FEM approach in the analysis of damage propagation under tensile load. It is a fundamental step in the understanding of damage-arresting capabilities that characterize the PRSEUS structural concept. Furthermore, a more challenging step would be the implementation of this study's work in a compressive model since Hashin failure criteria have long been proven to be difficult for predicting the onset and propagation of failure in panels subjected to a compressive load.

Data Availability

The data used to support the findings of this study are available from the authors upon request.

Conflicts of Interest

The authors declare that they have no conflicts of interest.

Acknowledgments

The authors disclosed receipt of the following financial support for the research, authorship, and/or publication of this article: this work was supported by the National Natural Science Foundation of China (Grant Nos. 11972301, 11201375, and 11972300), the Natural Science Foundation of Shaanxi Province (Grant No. 2018JQ1071), the State Key Laboratory of Structural Analysis for Industrial Equipment (China) (Grant No. GZ18107), and the Fundamental Research Funds for the Central Universities of China (Grant No. G2019KY05203).

References

[1] V. Li and A. Velicki, "Advanced PRSEUS structural concept design and optimization," in *Proceedings of the 12th AIAA/ISSMO Multidisciplinary Analysis and Optimization Conference*, Victoria, British Columbia, Canada, 2008.

[2] D. C. Jegley, A. Velicki, and D. A. Hansen, "Structural efficiency of stitched rod-stiffened composite panels with stiffener crippling," in *Proceedings of the 49th AIAA/ASME/ASCE/AHS/ASC Structures, Structural Dynamics and Materials Conference*, Schaumburg, IL, 2008.

[3] A. Velicki, P. Thrash, and D. C. Jegley, "Airframe development for the hybrid wing body aircraft," in *Proceedings of the 47th AIAA Aerospace Sciences Meeting Including the New Horizons Forum and Aerospace Exposition*, Orlando, Florida, 2009.

[4] N. P. Yovanof, A. Velicki, and V. Li, "Advanced structural stability analysis of a nonlinear, BWB-shaped vehicle," in *Proceedings of the 50th AIAA/ASME/ASCE/AHS/ASC Structures, Structural Dynamics and Materials Conference*, Palm Springs, California, 2009.

[5] A. Velicki and P. Thrash, "Advanced structural concept development using stitched composites," in *Proceedings of the 49th AIAA/ASME/ASCE/AHS/ASC Structures, Structural Dynamics and Materials Conference*, Schaumburg, IL, 2008.

[6] A. Velicki, *Damage Arresting Composites for Shaped Vehicles, Phase I Final Report*, NASA CR-2009-215932, NASA Langley Research Center, Hampton, VA, 2009.

[7] T. A. Reist and D. W. Zingg, "High-fidelity aerodynamic shape optimization of a lifting-fuselage concept for regional aircraft," *Journal of Aircraft*, vol. 54, no. 3, pp. 1085–1097, 2017.

[8] D. Jegley and A. Velicki, "Status of advanced stitched unitized composite aircraft structures," in *51st AIAA Aerospace Sciences Meeting including the New Horizons Forum and Aerospace Exposition*, pp. 1–12, Grapevine, Texas, 2013.

[9] P. Okonkwo and H. Smith, "Review of evolving trends in blended wing body aircraft design," *Progress in Aerospace Science*, vol. 82, pp. 1–23, 2016.

[10] R. H. Liebeck, "Design of the blended wing body subsonic transport," *Journal of Aircraft*, vol. 41, no. 1, pp. 10–25, 2004.

[11] C. Nickol and L. Mccullers, "Hybrid wing body configuration system studies," in *47th AIAA Aerospace Sciences Meeting including The New Horizons Forum and Aerospace Exposition*, pp. 1–12, Orlando, Florida, 2009.

[12] Z. Lyu and J. R. Martins, "Aerodynamic design optimization studies of a blended-wing-body aircraft," *Journal of Aircraft*, vol. 51, no. 5, pp. 1604–1617, 2014.

[13] H. D. Kim, J. L. Felder, M. T. Tong, J. J. Berton, and W. J. Haller, "Turboelectric distributed propulsion benefits on the N3-X vehicle," *Aircraft Engineering and Aerospace Technology*, vol. 86, no. 6, pp. 558–561, 2014.

[14] M. J. Czech, R. H. Thomas, and R. Elkoby, "Propulsion airframe aeroacoustic integration effects for a hybrid wing body aircraft configuration," *International Journal of Aeroacoustics*, vol. 11, no. 3-4, pp. 335–367, 2012.

[15] A. E. Lovejoy, *Optimization of Blended Wing Body Composite Panels Using Both NASTRAN and Genetic Algorithm*, NASA/CR-2006-214515, Hampton, VA, 2006.

[16] A. Velicki, N. P. Yovanof, J. Baraja et al., *Damage Arresting Composites for Shaped Vehicles—Phase II Final Report*, NASA CR-2011-216880, 2011.

[17] ABAQUS, *Version 6.10-1 on-Line Documentation, ABAQUS Analysis User's Manual*, Dassault Systemes Simulia Corp, Providence, RI, 2010.

[18] Z. Hashin and A. Rotem, "A fatigue failure criterion for fiber reinforced materials," *Journal of Composite Materials*, vol. 7, no. 4, pp. 448–464, 1973.

[19] Z. Hashin, "Failure criteria for unidirectional fiber composites," *Journal of Applied Mechanics*, vol. 47, no. 2, pp. 329–334, 1980.

[20] S. Poorasadion, *User subroutines in Abaqus*, 2015.

[21] "Title 14 Code of Federal Regulation, Part 25: Airworthiness standards: transport category airplanes, Subpart C "Structure," Sec. 25.305, Electronic Code of Federal Regulations," September 2013, http://www.ecfr.gov/cgi-bin/text-idx?c=ecfr&tpl=/ecfrbrowse/Title14/14cfr25_main_02.tpl.

[22] A. Przekop, "Repair concepts as design constraints of a stiffened composite PRSEUS panel," in *53rd AIAA/ASME/ASCE/AHS/ASC Structures, Structural Dynamics and Materials Conference*, Honolulu, Hawaii, 2012.

[23] A. Przekop and D. C. Jegley, "Evaluation of a metallic repair on a rod-stiffened composite panel," *Journal of Aircraft*, vol. 51, no. 3, pp. 792–804, 2014.

[24] S. Mirsamadi, *Advanced Subsonic Technology (AST) Composite Wing Material Stiffness and Allowable Strength Properties for Stitched Composite Laminates*, Boeing Company, Advanced Transport Aircraft Development, Rept. 98K0318, Long Beach, CA, 1998.

[25] F. Larbi Chaht, M. Mokhtari, and H. Benzaama, "Using a Hashin criteria to predict the damage of composite notched plate under traction and torsion behavior," *Frattura ed Integrìa Strutturale*, vol. 13, no. 50, pp. 331–341, 2019.

[26] F. Cepero-Mejias, V. A. Phadnis, and J. L. Curiel-Sosa, "Machining induced damage in orthogonal cutting of UD composites: FEA based assessment of Hashin and Puck criteria," *Procedia CIRP*, vol. 82, pp. 332–337, 2019.

[27] H. Fallahi, F. Taheri-Behrooz, and A. Asadi, "Nonlinear mechanical response of polymer matrix composites: a review," *Polymer Reviews*, vol. 60, no. 1, pp. 42–85, 2020.

[28] R. M. A. Khan, S. Saeidiharzand, I. Emami Tabrizi, H. Q. Ali, and M. Yildiz, "A novel hybrid damage monitoring approach to understand the correlation between size effect and failure behavior of twill CFRP laminates," *Composite Structures*, vol. 270, article 114064, 2021.

[29] G. G. Sheng and X. Wang, "Nonlinear forced vibration of functionally graded Timoshenko microbeams with thermal effect and parametric excitation," *International Journal of Mechanical Sciences*, vol. 155, pp. 405–416, 2019.

[30] B. C. Van Der Vossen and A. V. Makeev, "Mechanical properties characterization of fiber reinforced composites by nonlinear constitutive parameter optimization in short beam shear specimens," *Journal of Composite Materials*, vol. 55, no. 21, pp. 2985–2997, 2021.

[31] A. Przekop, "Design and analysis of a stiffened composite structure repair concept," in *52nd AIAA/ASME/ASCE/AHS/ASC Structures, Structural Dynamics and Materials Conference*, Denver, Colorado, April 2011.